Pre-Synaptic Inhibition of Afferent Feedback in the Macaque Spinal Cord Does Not Modulate with Cycles of Peripheral Oscillations Around 10 Hz

Ferran Galán and Stuart N. Baker *

Movement Laboratory, Institute of Neuroscience, Newcastle University, Newcastle Upon Tyne, UK

Spinal interneurons are partially phase-locked to physiological tremor around 10 Hz. The phase of spinal interneuron activity is approximately opposite to descending drive to motoneurons, leading to partial phase cancellation and tremor reduction. Pre-synaptic inhibition of afferent feedback modulates during voluntary movements, but it is not known whether it tracks more rapid fluctuations in motor output such as during tremor. In this study, dorsal root potentials (DRPs) were recorded from the C8 and T1 roots in two macaque monkeys following intra-spinal micro-stimulation (random inter-stimulus interval 1.5–2.5 s, 30–100 μA), whilst the animals performed an index finger flexion task which elicited peripheral oscillations around 10 Hz. Forty one responses were identified with latency <5 ms; these were narrow (mean width 0.59 ms), and likely resulted from antidromic activation of afferents following stimulation near terminals. Significant modulation during task performance occurred in 16/41 responses, reflecting terminal excitability changes generated by pre-synaptic inhibition (Wall's excitability test). Stimuli falling during large-amplitude 8–12 Hz oscillations in finger acceleration were extracted, and sub-averages of DRPs constructed for stimuli delivered at different oscillation phases. Although some apparent phase-dependent modulation was seen, this was not above the level expected by chance. We conclude that, although terminal excitability reflecting pre-synaptic inhibition of afferents modulates over the timescale of a voluntary movement, it does not follow more rapid changes in motor output. This suggests that pre-synaptic inhibition is not part of the spinal systems for tremor reduction described previously, and that it plays a role in overall—but not moment-by-moment—regulation of feedback gain.

Keywords: primary afferent depolarization, pre-synaptic inhibition, tremor, afferent feedback, spinal cord

INTRODUCTION

Physiological tremor is produced by multiple interacting mechanisms. These include mechanical resonance of limb articulations (Marsden et al., 1969), and oscillations in the stretch reflex loop consequent on the peripheral conduction delays (Lippold, 1970). However, there is also a centrally generated component in the 8–12 Hz frequency range, as its frequency is unaltered by

manoeuvers such as loading the limb, which alter mechanical and reflex resonant frequencies (Elble and Randall, 1978). Studies assessing slow finger movements in non-human primates have found coherence at ∼10 Hz between acceleration and the activity of multiple motor structures during both active movements and periods of steady holding (Williams et al., 2010), suggesting that physiological tremor and discontinuities during slow finger movements reflect the same underlying phenomenon. Interestingly, motor cortical oscillations at ∼10 Hz are not coherent with muscle activity in this range during steady holding (Conway et al., 1995; Baker et al., 1997; Salenius et al., 1997) despite their passage down the corticospinal tract (Baker et al., 2003). These observations have suggested the existence of an active neural filter, which removes ∼10 Hz components from the input to motoneurons (Williams and Baker, 2009; Williams et al., 2010), that could be important in the reduction of tremor.

Spinal networks could influence motoneurons by multiple possible pathways, most obviously by excitatory or inhibitory synapses on the motoneurons themselves. One known instance of such a direct synaptic effect is Renshaw cell recurrent inhibition, which previous work has shown can partially cancel ∼10 Hz components in motoneuron input (Williams and Baker, 2009). However, spontaneous oscillations in the cord are also synchronized with similar oscillations in dorsal root potentials (DRPs; Lidierth and Wall, 1996), and are associated with primary afferent depolarization (PAD; Manjarrez et al., 2000) which reflects pre-synaptic inhibition of afferent input. It is not known whether these spontaneous spinal oscillations in anesthetized animals are related to tremor circuits. Furthermore, it is known that muscle spindle afferents modulate their discharge with the phases of peripheral oscillations around 10 Hz (Wessberg and Vallbo, 1995; Baker et al., 2006), and that pre-synaptic inhibition modulates during voluntary movements (Hultborn et al., 1987; Seki et al., 2003), suppressing motor oscillations during forelimb movement (Fink et al., 2014).

Given the above background, we hypothesized that presynaptic inhibition might modulate with the phase of ∼10 Hz oscillations in tremor. If the phase of such modulation were appropriate, this could lead to partial cancelation of oscillations in afferent activity, smoothing out the peaks and troughs and reducing the afferent contribution to tremor amplitude. However, such a timescale of modulation of pre-synaptic inhibition would be an order of magnitude faster than that reported previously during task performance in awake animals.

Using a new technique that allowed recordings from a mixed population of muscle and cutaneous afferents in awake behaving primates, this study investigated whether afferent axon terminal excitability modulates during performance of a slow index finger flexion task, and with the cycles of physiological tremor which are prominent in such a task. Although robust modulation over the second-to-second timescale of task performance was regularly seen, the data contained no evidence for faster modulation during the tremor cycle. These results suggest that pre-synaptic inhibition may act as a less temporally-precise gate for afferent inflow, but does not sculpt sensory input and its reflex consequences over timescales comparable to endogenous oscillations in motor output.

MATERIALS AND METHODS

Behavioral Task

Two female *Macaca mulatta* monkeys (denoted I and V) were trained to perform a finger flexion task for food reward, similar to that used in previous work (Williams et al., 2009, 2010; Soteropoulos et al., 2012). The index finger of the right hand was inserted into a narrow tube, which restricted movement to the metacarpophalangeal (MCP) joint. The tube was attached to a lever that rotated coaxially with the MCP joint (**Figure 1A**, Top); a motor exerted torque in a direction to oppose flexion. Lever angular displacement was sensed by an optical encoder and fed back to the animal via a cursor on a computer screen. A displacement of 0° indicated the neutral position, where the finger was in the same plane as the palm. Positive angles denoted finger flexion. During each trial the palm and digits 1, 3, 4, and 5 lay horizontally against a flat surface and the elbow and upper arm were held in a sleeve. The contralateral arm was unrestrained, and remained at rest during task performance; at the end of a successful trial, the contralateral arm retrieved the food reward.

For both animals, a trial commenced when a rectangular target appeared at 8° displacement. The animal moved the cursor into this target, which then moved over a linearly increasing displacement (ramp). In monkey I, the ramp phase lasted 1.5 s, with final displacement 20°; the trial was completed at the end of the ramp phase. In monkey V, the ramp phase lasted 2 s, with final displacement 16°; at the end of the ramp, there was a hold phase of constant target displacement lasting 1 s. Maintenance of the cursor within the target (allowed error ±1.4°) led to a food reward. An accelerometer attached to the lever measured movement discontinuities during the target ramp (band-pass, 1–100 Hz).

Surgical Preparation

Following training, both animals were implanted under general anesthesia (3.0–5.0% sevoflurane inhalation, intravenous infusion of 0.025 mg·kg^{-1}·h^{-1} alfentanil) and aseptic conditions with a stainless steel headpiece for head fixation. After an appropriate recovery period, a further surgery implanted a spinal chamber over a laminectomy spanning vertebrae C5-C7, together with a bipolar cuff electrode on the C8 (monkey I) or T1 (monkey V) dorsal root adjacent to the cord. This cylindrical cuff electrode was modeled on those commonly used for peripheral nerve stimulation and recording. It was manufactured from flexible medical-grade silicone polymer to have an internal diameter of 2.0 mm and length 5 mm. The cuff contained two platinum electrodes which ran around the internal circumference (electrode width 1.0 mm, separation 1.5 mm), and were spot-welded to Teflon-insulated stainless steel wire (wire diameter 150 μm). The dorsal root was inserted into the cuff via a slit along the length of the cuff, which was

then closed using two silk sutures which ran around the outside. Cuff placement was made possible by the fact that in monkey the C8/T1 roots run parallel to the cord for some distance before turning to exit the facet joint. This displacement between spinal segment and equivalent vertebra is much more marked in monkey than in man, where roots do not run parallel to the cord in this way until the mid-throracic level. The wires were run over the lateral mass and then up the side of the chamber, where they terminated in a connector. Both wires and connector were covered in dental acrylic for protection. Several features of the cuff design were intended to record selectively from the dorsal root, whilst reducing potentials from the adjacent cord. Firstly, the electrodes were closely spaced within an insulating cylinder, with the distance from each electrode to the cuff edge similar to the inter-electrode spacing. Secondly, the cuff lay parallel to the cord, so that each electrode was equidistant from any cord generators. We would therefore expect that any residual potentials from the cord would be similar on each electrode, and hence cancel in the differential recording.

Post-operative care after all surgeries included analgesia (meloxicam, 0.07 mg/kg oral suspension daily for 5–10 days; buprenorphine, 0.24 mg/kg IM, given only if required for up to 2 days; Duragesic fentanyl patch after spinal implant only in monkey I, for 4 days), steroid anti-inflammatory treatment (dexamethasone, 0.32 mg/kg IM daily for 2–4 days) and antibiotic cover (cefalexin 9 mg/kg IM once daily, or amoxicillin (Clamoxyl LA), 15 mg/kg once daily, both for a 10 day course). All procedures were performed under appropriate licenses issued by the UK Home Office under the Animals (Scientific Procedures) Act (1986) and were approved by the Animal Welfare and Ethical Review Board of Newcastle University.

Recordings

During task performance both head and spinal implants were fixed to the primate chair and a microdrive was interfaced to the spinal chamber via an X-Y positioning stage. Differential recordings from the contacts of the dorsal root cuff electrodes yielded the dorsal root potential (DRP, band pass 3 Hz–2 kHz, gain 50 K). Intraspinal microstimulation (ISMS; bipolar pulses, 0.07–0.1 ms per phase, inter-stimulus interval chosen at random from a uniform distribution in the range 1.5–2.5 s, 30–100 μA) was delivered through a tungsten microelectrode (impedance 1 MΩ) inserted into the spinal gray matter at a location which evoked responses in the DRP (see **Figure 1**). Electrode depth ranged 2.0–7.2 mm relative to the surface of the dura mater (mean 5.1 mm, SD 1.2 mm). Stimulus intensity was set to yield response amplitudes around half of the maximum. Stimulus timing was controlled by a 1401 interface (CED Ltd, Cambridge, UK), which also recorded DRP (sampling rate 20 kHz), lever position and acceleration (sampling rate 1 kHz) and task markers to disk for later off-line analysis.

Dorsal root responses following ISMS had a complex profile. In order to clarify the origin of the different components, these were compared with responses following median nerve stimulation (1 ms bipolar pulses, 1–3 Hz, 0.4–1.8 mA applied to surface electrodes at the wrist) in both the dorsal root cuff and the spinal cord (recorded by a tungsten microelectrode as above, band pass 1 Hz–5 kHz, gain 2 K, sampling rate 10 kHz; **Figure 2**).

Modulation of ISMS Evoked Responses at Dorsal Root

Evoked responses in the DRP following ISMS were first determined by averaging triggered by all stimuli delivered to a given spinal site. This allowed estimation of the peak-to-peak amplitude of each component, measured over a time window selected manually. The latency was estimated from the time of the first peak of that component.

To estimate the task-dependent modulation of responses, trials were first aligned to the end of the ramp phase of the task. Stimuli were then sorted depending on when they had occurred relative to this alignment point, into 26 non-overlapping bins, each 200 ms wide, spanning from 3 s before to 2 s after the end of the ramp. Selective averages were compiled of stimuli in each bin, and amplitude measured from each average using the time window defined from the all-stimulus average.

To estimate how evoked responses modulated with tremor phase, stimuli were first selected using two criteria. It is known that peripheral oscillations are stronger during periods of finger movement (which motivated our use of a task incorporating a ramp phase). Accordingly, the finger lever velocity V was estimated over a window prior to the stimulus at time T as:

$$V(t) = \frac{x(T) - x(T-\tau)}{\tau} \quad (1)$$

Where, x represents the lever displacement, and the window length τ was set to 100 ms. The amplitude spectrum of the lever acceleration was estimated over a window prior to the stimulus at time t (where $t < 0$) using non-symmetric causal wavelets as described in Mitchell et al. (2007). In brief, the wavelet W at frequency f was defined as the product of an alpha function with peak $0.8/f$ before the stimulus, with a complex sinusoid:

$$W^f(t) = -\frac{5ft}{4} e^{\left(2\pi fti + \frac{5ft}{4}\right)} \quad (2)$$

For a given frequency f, a section of accelerometer signal S was extracted lasting seven oscillation periods prior to the stimulus at time T. The dot-product of the accelerometer signal S with the wavelet W^f was found:
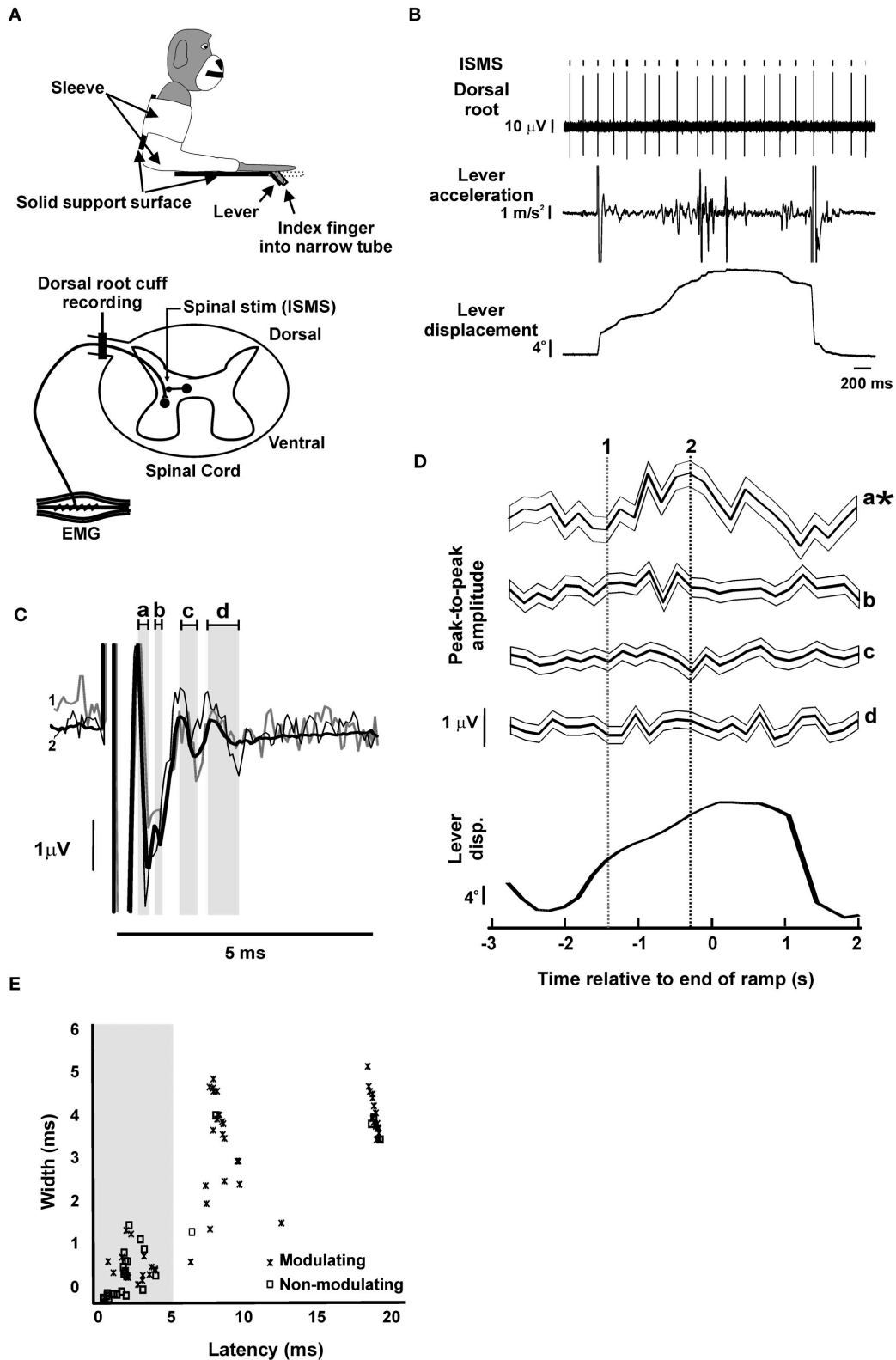
$$D^f = \int_{t=-7/f}^{0} W^f(t) S(t+T) \, dt \quad (3)$$

The amplitude A and phase φ were measured as:

$$A^f = \left| D^f \right|$$

$$\phi^f = arctan\left(\frac{Im\left\{D^f\right\}}{Re\left\{D^f\right\}}\right) \quad (4)$$

Only stimuli with V > 15°/s and which had the bin with largest spectral power lying within the 8–12 Hz range were

FIGURE 1 | Dorsal root potentials evoked by intra-spinal micro-stimulation (ISMS). (A) Schematics of behavioral task and recording setup. Top, the monkey arm was held in a sleeve and the index finger of the right hand was inserted into a narrow tube, restricting the movement to the MCP joint. The tube was attached to a

(Continued)

lever that rotated coaxially with the MCP joint. Bottom, a bipolar cuff electrode was implanted on the C8 or T1 dorsal root adjacent to the spinal cord. During task performance, ISMS was delivered at a location which elicited antidromic responses in the mixed population of afferents recorded at the dorsal root electrode. **(B)** Example raw data during task performance. **(C)** Example of responses evoked at the dorsal root by ISMS to a single spinal site (65 μA). Thick black trace represents grand-average (n = 4698 stimuli); thin black and thin gray traces represent sub-averages from task-dependent bins marked by dotted lines in **(D)**. Gray shading and lower case letters indicate different response components. **(D)** Task-dependent modulation of the responses indicated by lower case letters in **(C)**. Each trace shows the mean response, with faint surrounding traces indicating the SEM. Traces are aligned to the end of the ramp phase of the task; average lever displacement is shown below in the same timeframe for comparison. Asterisks denote responses with significant task-dependent modulation. Vertical lines indicate times used to compute sub-averages illustrated in **(C)**. **(E)** Scatter plot of the width vs. latency of responses (n = 88). Only responses with latency shorter than 5 ms (gray shading) were used in subsequent analysis (n = 41). Panel **(A)** is modified with permission from Soteropoulos et al. (2012).
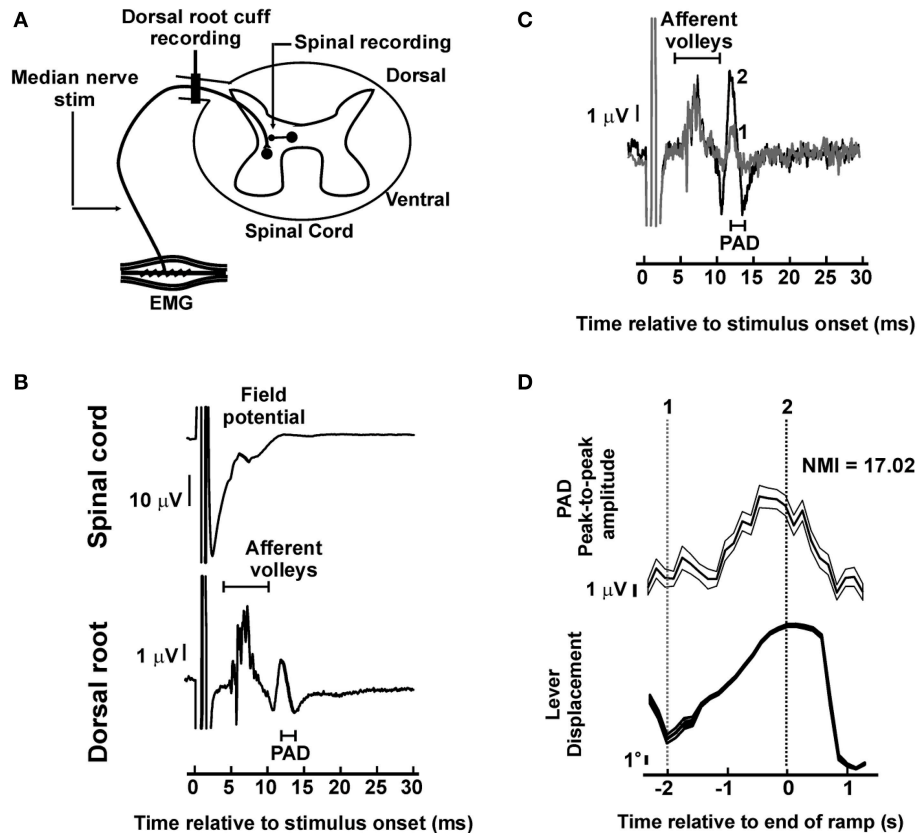
FIGURE 2 | Dorsal root potentials evoked by peripheral nerve stimulation. (A) During task performance the median nerve was stimulated whilst recordings were made from the dorsal root and the spinal cord. **(B)** Example of averaged responses in one experiment. In the dorsal root potential, an early afferent volley is followed by later primary afferent depolarization potential (PAD). In the spinal cord, the field potential developed at latencies intermediate between the early afferent volleys and PAD in dorsal root. Thick black trace represent grand-average (n = 10859 stimuli). **(C)** Dorsal root potentials during task performance, black and gray traces represent sub-averages from the times indicated in **(D)**. **(D)** Significant task-dependent modulation of the amplitude of the PAD potential shown in **(B,C)**. Top trace is mean PAD amplitude (thick line) and its SEM (thin line). Bottom trace is the average lever displacement, in the same timeframe, for reference. Vertical dotted lines indicate time points used for the corresponding sub-averages in **(C)**.

included for subsequent analysis of tremor modulation. Note that using these criteria, stimuli falling in unsuccessful trials (e.g., where the animal strayed outside the imposed limits on tracking performance toward the end of a trial) were able to be used as well as those during successful task performance.

Stimuli which survived this pre-selection were then grouped by the phase of on-going lever acceleration oscillations in which they occurred, using eight equally-sized bins from 0 to 2π. DRP averages were then compiled selectively from stimuli in each bin,

and response amplitude measured for each sub-average as for the determination of task modulation. Because the wavelet analysis of Equation (3) used only acceleration data before the stimulus, any consequence of the stimulus on the periphery (such as a twitch) could not affect the phase determination. Inter-stimulus intervals were chosen at random (range 1.5–2.5 s) to prevent phase-locking of oscillations to the stimulus.

Plots of response amplitude vs. bin number often showed complex patterns of modulation, for both task and phase

dependent modulation. A simple summary measure, which quantified the overall extent of this modulation in a single number, was developed. First, a raw modulation index from the experimental data, I_{exp}, was computed as

$$I_{exp} = \sum_{n=1}^{N} \left| A_n - \overline{A} \right| \qquad (5)$$

Where A_n, is the response amplitude measured in bin n. The number of bins N was 26 for task modulation and 8 for tremor. The mean response $\overline{A}$ was calculated as:

$$\overline{A} = \frac{1}{N} \sum_{n=1}^{N} A_n \qquad (6)$$

The measure I quantifies how much single bin responses deviate from the average response, but it is difficult to interpret the scale of this number. Accordingly, surrogate datasets were generated, which estimated how great I would be, on the null hypothesis of no response modulation above that expected by chance fluctuations. Surrogates were compiled by randomly shuffling bin assignments of individual stimuli; for a given bin, the number of stimuli assigned to it was fixed equal to the number in the experimentally determined dataset. Sub-averages were compiled for the surrogate data, and the measure I recompiled. This was repeated 500 times, using different random assignments of stimuli to bins. The mean $\overline{I}$ and standard deviation σ_I of the surrogate values of I was found, allowing us to compute a normalized modulation index (NMI_{exp}) as:

$$NMI_{exp} = \frac{I_{exp} - \overline{I}}{\sigma_I} \qquad (7)$$

If I_{exp}, exceeded the 95th percentile of the surrogate values of I, the modulation was considered to be statistically significant ($P < 0.05$).

To interpret the scale of tremor modulation in the 8–12 Hz range further and be able to compare it with other frequency ranges, data were combined across recording sites in two ways, estimating both the count C of significantly tremor-modulating responses, and also the mean modulation index $\overline{NMI}$ across all sites. Surrogate measures of C and $\overline{NMI}$ were generated by counting or averaging over one surrogate value of I per site; this was repeated 500 times with different randomly generated surrogates. If C_{exp} and $\overline{NMI}_{exp}$ from the experimental data exceeded the 95th percentile of the surrogate values, they were considered to be statistically significant ($P < 0.05$). This whole procedure was repeated for frequencies between 6 and 50 Hz (1 Hz resolution).

Identification of Task-dependent Modulation Patterns of ISMS Evoked Responses at Dorsal Root

It is of interest to determine whether responses with a significant task-dependent modulation from different spinal sites could be grouped into a smaller number of representative profiles. Profiles were accordingly subjected to unsupervised k-means clustering (Jain, 2010), using the correlation between profiles of amplitude

vs. bin number as the metric of pairwise distance. The number of identified patterns (=number of clusters, s) was chosen by maximizing the relatedness of the modulating responses across solutions for s=1…10. Response relatedness was estimated using the intra-cluster correlation coefficient:

$$ICC(s) = \frac{\overline{Corr}_{within}}{\overline{Corr}_{within} + \overline{Corr}_{between}} \qquad (8)$$

Where, $\overline{Corr}_{within}$ is the average squared correlation within clusters, and $\overline{Corr}_{between}$ is the average squared correlation between clusters. Given a clustering solution s with clusters indexed by c or $d = 1..s$, and each cluster containing n_c responses $Resp_j^c$ ($j = 1..n_c$), $\overline{Corr}_{within}$ and $\overline{Corr}_{between}$ were calculated as:

$$\overline{Corr}_{within} = \frac{1}{n_c s} \sum_{c=1}^{s} \sum_{j=1}^{n_c} Corr(Resp_j^c, Centroid_c)$$

$$\overline{Corr}_{between} = \frac{1}{s^2} \sum_{c=1}^{s} \sum_{d=1}^{s} Corr(Centroid_c, Centroid_d)$$
$$(9)$$

Where, $Corr(Resp_j^c, Centroid_c)$ is the squared correlation between a response $Resp_j^c$ and the centroid of parent cluster, and $Corr(Centroid_c, Centroid_d)$ is the squared correlation between centroids of clusters c and d.

Values of ICC_s close to one reflect solutions where responses are very similar within a cluster, but unrelated to those in another cluster. Estimates of ICC_s were produced using leave-one-out cross-validation, in which each response was correlated with cluster centroids determined after excluding that response from the dataset.

All analysis routines were implemented in the MATLAB package (The MathWorks Inc, Natick, MA, USA).

RESULTS

Responses Evoked in Dorsal Root Recordings by ISMS

Results were available from stimulation at a total of 21 spinal sites (8 monkey I, 13 monkey V). At each site, between 392 and 29516 stimuli were delivered (mean stimulus intensity 82 μA, SD 64 μA), whilst the animal performed between 20 and 161 successful trials of the task.

Figure 1B illustrates typical raw data from an experiment, and **Figure 1C** shows the averaged DRP evoked by the ISMS (stimulus intensity 65 μA, depth 4.4 mm). A complex waveform was visible in this average, reflecting multiple components of the response which are identified by the gray shading labeled with lower case letters.

Figure 1D shows how the different parts of the response from **Figure 1C** modulated with task performance. Each trace shows the amplitude of one component as a function of time during the task (see averaged lever displacement beneath as a reference); traces illustrate both averaged amplitude (thick lines) and the corresponding standard error of the mean (thin lines). The earliest response (a) exhibited significant modulation

with task, and the corresponding NMI value was above the 95th percentile of those in surrogate datasets (experimental/95th centile surrogate NMI: 2.0/1.6). By contrast, later responses (b, c, d) had NMI below those expected by chance from surrogate data (b, 1.2/1.6; c, 1.3/1.8; d, 0.5/1.9), indicating no significant modulation with task.

Across all 21 spinal sites which were stimulated, a total of 88 distinct responses were identified in the DRP, 57 of which (65%) modulated significantly with the task. In order to provide some insight into the physiological mechanisms generating the different response components, **Figure 1E** plots their width (peak-trough time) vs. latency (time of earliest peak/trough); components which modulated significantly with task are identified by crosses. It is clear that there are three broad classes of response. The earliest components (latency <5 ms; mean 2.44 ms, SD 1.15 ms) were narrow (width 0.59 ± 0.45 ms, mean ± SD), and contained a mixture of modulating (16/41) and non-modulating (25/41) effects. The narrow nature of these responses suggests that these are most likely to reflect antidromic action potentials generated by direct stimulation of afferent axons within the cord. Such effects could exhibit a task relationship if the stimulating electrode was close to axon terminals, and those terminals were depolarized by axo-axonic synapses mediating primary afferent depolarization (PAD; Wall, 1958), thereby modulating their excitability to the stimulus.

There appeared to be two later clusters of responses, with mean latencies of 8.1 and 18.1 ms. These, showed a greater incidence of task-dependent modulation (22/24 and 19/23 responses, respectively); both groupings of response were broader (widths 3.3 ± 0.1 and 4.1 ± 0.1 ms, respectively). One possible cause for these effects could be PAD elicited in afferent axon terminals following activation of spinal neurons by the stimulus (either directly, or trans-synaptically), and passively conducted to the dorsal root recording site (Wall, 1958). For the latest responses, it is possible that they are caused by reafference following a peripheral twitch induced by the ISMS.

Comparison with Responses Evoked in Dorsal Root Recordings by Peripheral Nerve Stimulation

Further insight into the mechanisms generating the later DRPs described above was provided by examining the responses to peripheral nerve stimulation (**Figure 2A**). **Figure 2B** shows the average response after stimulation of the median nerve at the wrist, at an intensity above motor threshold that did not interfere with task performance (1.4 mA), for a single recording session. The DRP recording showed a compound volley, which has a first peak latency 3.9 ms after the stimulus. This contained multiple sharp components, presumably reflecting axons of different conduction velocities, and was followed by a slower potential (width peak-to-peak 1.0 ms), with first peak at 10.1 ms after the stimulus. We consider that this component is likely to reflect PAD (see Discussion). In the spinal cord, field potential onset was measured 4.2 ms after the stimulus.

Figures 2C,D illustrates that this later potential modulated strongly with task performance, indicating that the excitability of

neural populations mediating PAD changed in a task-dependent manner. Significant task-dependent modulation of a potential similar to that seen in **Figure 2B** was observed in 3/4 recording sessions where median nerve stimulation was tested (NMI values 12.3, 5.0, and 17.0; probability of three or more out of four significant values by chance is $P < 5 \times 10^{-5}$, binomial distribution).

In these three sessions, the average latency difference between the earliest afferent volley and the later PAD potential was 5.1 ± 0.58 ms; the width of the later PAD potential was 1.1 ± 0.05 ms (both mean ± SEM). The latency is comparable to the later potentials seen following ISMS in **Figure 1E**, although those elicited by afferent input were considerably narrower. It is possible that changes in terminal membrane conductances following prior activation by the afferent volley interacted with the PAD to reduce its width. The responses to median nerve stimulation therefore seem broadly to support the idea that the later responses to ISMS reflect PAD elicited by activation of spinal neurons.
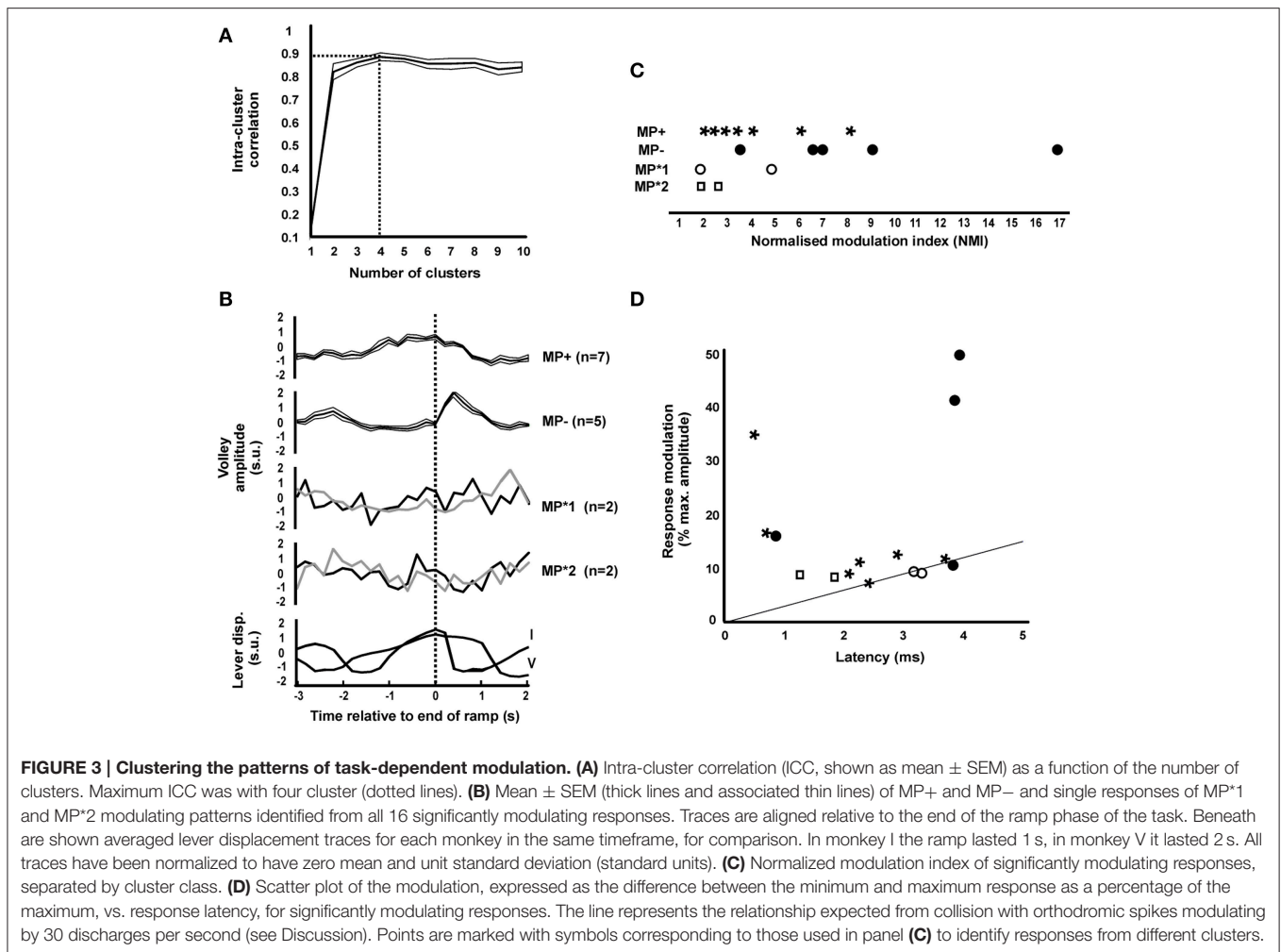
Patterns in the Task-dependent Modulation of ISMS-evoked Dorsal Root Responses

A k-means clustering approach was used to examine whether there were any repeatable patterns in the task modulation profiles of the short-latency (<5 ms) ISMS responses from different sites (see Materials and Methods). A plot of the intra-cluster correlation (**Figure 3A**) revealed a sharp increase in going from one to two clusters, but then only a small increase as the cluster number was further increased, peaking at four clusters. **Figure 3B** presents information on the different profiles identified. Of the 16 responses with significant modulation, seven showed response facilitation during the task ramp phase (MP+), while five showed a facilitation just after the ramp phase ended (MP−). The remaining two clusters appeared to have erratic profiles and were categorized as MP*1 and MP*2 (n = 2 sites each). Averaged lever displacement traces are shown at the bottom in **Figure 3B**, and make clear that there were differences in the temporal profile of task performance between the two animals. Interestingly, the modulation profiles MP+, MP*1, and MP*2 all occurred in monkey V, whereas MP− profiles all occurred in monkey I, suggesting that individual differences in the task and its performance lay behind the modulation differences. There was no significant difference between the modulation depths of the four patterns (**Figure 3C**; $P = 0.104$, Kruskal–Wallis test).

Figure 3D presents the relation of the size of the modulation in response (calculated as the difference between minimum and maximum response, as a percentage of the maximum) with response latency. The straight line indicates the largest modulation which we estimate could be generated by collision between orthodromic and antidromic spikes; more detail on the basis for the calculation of this line and the implications of this plot are given in the Discussion.

Modulation of ISMS Evoked Dorsal Root Responses with Tremor Cycle

Figure 4A illustrates typical raw data from an experiment, marking with vertical dotted lines the stimuli which were

FIGURE 3 | Clustering the patterns of task-dependent modulation. (A) Intra-cluster correlation (ICC, shown as mean ± SEM) as a function of the number of clusters. Maximum ICC was with four cluster (dotted lines). **(B)** Mean ± SEM (thick lines and associated thin lines) of MP+ and MP− and single responses of MP*1 and MP*2 modulating patterns identified from all 16 significantly modulating responses. Traces are aligned relative to the end of the ramp phase of the task. Beneath are shown averaged lever displacement traces for each monkey in the same timeframe, for comparison. In monkey I the ramp lasted 1 s, in monkey V it lasted 2 s. All traces have been normalized to have zero mean and unit standard deviation (standard units). **(C)** Normalized modulation index of significantly modulating responses, separated by cluster class. **(D)** Scatter plot of the modulation, expressed as the difference between the minimum and maximum response as a percentage of the maximum, vs. response latency, for significantly modulating responses. The line represents the relationship expected from collision with orthodromic spikes modulating by 30 discharges per second (see Discussion). Points are marked with symbols corresponding to those used in panel **(C)** to identify responses from different clusters.
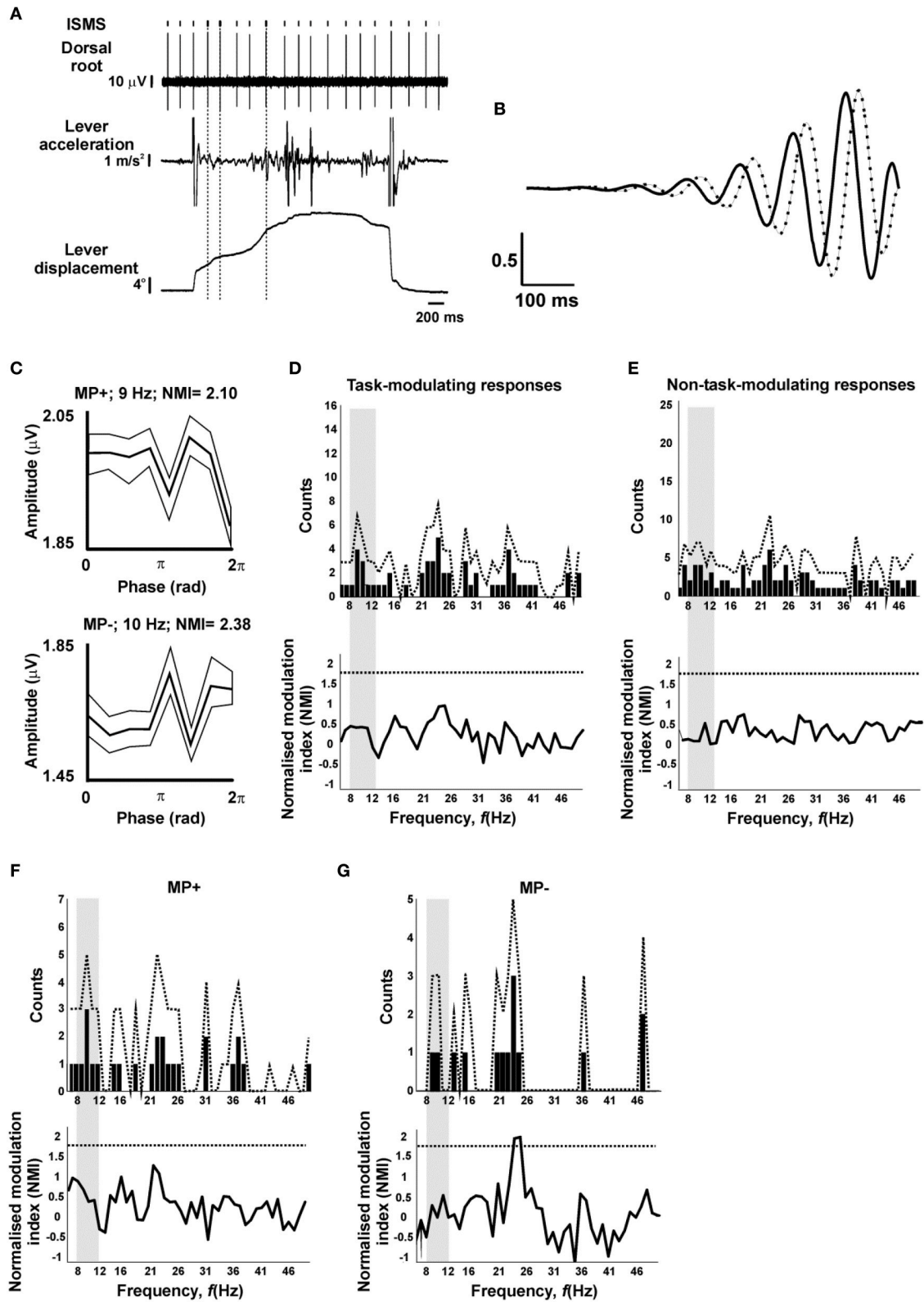
included for analysis of tremor modulation based on a linearly increasing lever displacement and a power spectral peak of lever acceleration in the 8–12 Hz range. **Figure 4B** shows the asymmetric wavelet used to extract amplitude and phase information from the acceleration signal (see Materials and Methods). **Figure 4C** shows two example phase-dependent modulation profiles of responses classified as MP+ and MP− on the basis of task. Each of these had NMI values above those expected by chance from surrogate data, indicating a significant modulation with tremor oscillatory phase at the frequencies illustrated (9 and 10 Hz, respectively).

To examine whether this modulation in the ∼10 Hz tremor range was above that expected by chance and whether it reflected the specific involvement of presynaptic inhibition in regulating these frequencies, the count of significantly modulating responses and the average modulation depth across the 6–50 Hz frequency range (1 Hz resolution; see Materials and Methods) was evaluated. This is illustrated in **Figure 4D**, for responses which modulated significantly with task; experimental values are shown with bars, together with the 95th percentile of surrogate data with dotted traces. Neither the number of

modulating responses, nor the mean modulation index exceeded the bounds expected by chance, at any of the frequencies tested. **Figure 4E** repeats this analysis for those responses which did not show a significant task-dependent modulation; once again, no significant modulation with tremor was detected.

In the case of the task-modulating responses of **Figure 4D**, it is conceivable that pooling responses with different task-modulating profiles has obscured a significant modulation at the sub-population level. To explore this in more detail, the phase-dependent analysis was stratified by considering responses with MP+ and MP− modulating profiles separately (MP*1 and MP*2 were excluded due to their small sample size; $n = 2$ sites each). The count of modulating sites did not rise above the bounds expected by chance for either profile at any frequency (**Figures 4F,G**, top traces). For the average modulation index in MP− responses, 2/45 frequency bins exceeded the 95th percentile of the surrogate data, at 24 and 25 Hz. However, two or more frequency bins are expected to exceed the $P < 0.05$ significance level merely by chance 45% of the time (surrogate distribution), therefore such modulation is not statistically significant.

FIGURE 4 | Lack of tremor-dependent modulation. (A) Example raw data during task performance. Vertical dotted lines indicate stimuli which passed the criteria for inclusion in analysis of tremor modulation (lever velocity>15°/s, lever acceleration power spectral peak in the 8–12 Hz range). **(B)** Asymmetric wavelet used to

(Continued)

FIGURE 4 | Continued
determine phase of oscillations in lever acceleration; both real (solid) and imaginary (dotted) components are shown. **(C)** Example tremor modulation profiles of antidromic responses categorized on the basis of their task modulation as MP+ or MP−. Each trace shows the mean (thick line) and SEM (thin lines) of the response amplitude as a function of oscillation phase. **(D)** Number of responses which showed significant modulation with phase, as a function of frequency (top), and the mean normalized modulation index (NMI, bottom), for responses with a significant task-dependent modulation. **(E)** as **(D)**, but for responses without significant task-dependent modulation. **(F,G)**, as **(D)**, but only for responses categorized as MP+ **(F)** or MP− **(G)** on the basis of their task-dependent modulation. In **(D–G)**, dotted lines indicate significance limits; traces must cross these to achieve significance ($P < 0.05$) for an individual bin. Gray shading indicates the 8–12 Hz range relevant to peripheral tremor.

DISCUSSION

In this work we have provided evidence that pre-synaptic inhibition does not show moment-by-moment modulation with the phase of physiological tremor, although by contrast it does modulate on the slower timescales of behavioral task performance. In the following, we first consider details of our methods and how they may have influenced the results, before discussing the broader significance of the findings.

Physiological Mechanism Underlying Recorded Potentials

We propose that the narrow, early responses seen in the DRPs were probably generated by antidromic action potentials following stimulation of afferent axons within the spinal cord. Such responses are known to modulate if the stimulation site is close to axon terminals, because depolarization of the terminals during pre-synaptic inhibition changes their excitability (Wall, 1958). Instances where these early responses did not modulate with task could reflect either terminals which do not receive task-dependent PAD, or situations where the stimulating electrode activated stem axons, distant from the terminals and hence with a constant level of excitability. In addition, it is possible that multiple axons were activated, and that their modulation profile differed so that the modulation canceled in the compound volley to become negligible. It is known that individual axons can show highly specific patterns of pre-synaptic inhibition; even different terminals of the same axon may show different effects (Lomelí et al., 1998; Rudomin et al., 2004). However, before accepting this explanation of the likely generator of these early potentials, we must first consider their latency, which initially appears longer than expected. Measurements from photographs taken during the implant surgery of monkey V suggested a conduction distance from the point where the dorsal root leaves the cord to the first contact of the cuff electrode of 5.3 mm. Measurements from spinal sections indicated an approximate conduction distance from dorsal root to intermediate zone of 2.7 mm. Using this total conduction distance of $5.3 + 2.7 = 8.0$ mm, an onset latency of 2.4 ms would imply a very slow conduction velocity of 3.3 m/s, well below accepted values for the fast cutaneous and proprioceptive afferents which are the target in these experiments. It seems unlikely that the weak ISMS ($\leq 100 \, \mu$A) delivered in these experiments could activate such slowly conducting fibers. This is supported by the behavioral reaction of the animals to these stimuli; aside from the usual brief orienting response to a stimulus, the monkeys quickly adapted

and showed no signs of pain or irritation, which would be expected if we activated slow, presumed nociceptive fibers.

Several factors probably conspire to make the observed conduction longer than the naïve expectation based on conduction distance divided by expected conduction velocity. One must allow for an utilization time of 0.1 ms, and for an additional delay due to slow conduction within the intraspinal axon terminal. For corticospinal axons, Shinoda et al. (1986) showed that the conduction velocity within terminal branches could be as low as 1 m/s. Assuming similar slowing at peripheral axon terminals, this would introduce an additional latency of around 1 ms (Shinoda et al., 1986; Baker and Lemon, 1998). A further problem is that the stimulus artifact may obscure the earliest part of a response. The latencies of the visible peaks or troughs which we measure may therefore be later than the true onset latency by up to 0.5 ms (the width of an axonal action potential, Marks and Loeb (1976)). For the mean latencies observed of 2.4 ms, these considerations suggest that the conduction time in the stem axon may be only 0.8 ms, which would correspond to a velocity of 10 m/s. Finally, Loeb (1976) demonstrated that for a given axon, the conduction velocity in the dorsal root is on average 43% of that in the peripheral nerve, but this factor showed considerable variation from 20 to 70%. At the limit, a root velocity of 10 m/s would then correspond to a peripheral velocity of 50 m/s, at the upper end of the Group II range (Cheney and Preston, 1976). For comparison, Seki et al. (2009) delivered ISMS and recorded volleys in the purely cutaneous superficial radial nerve peripherally; they estimated conduction velocities of 20–90 m/s, with a mean around 60 m/s. They did not correct for terminal branch and dorsal root slowing as described above in calculating these velocities, but the error is likely to have affected their readings proportionately less as their preparation had a substantially larger conduction distance (around 240 mm based on values in their Figure 7). We conclude that the latencies of the early responses in these recordings are consistent with antidromic conduction in fast myelinated axons. It is not possible, however, to specify the nature of the axonal population; it is likely to contain a mixture of afferents responsive to both cutaneous and deep receptors.

Previous work on DRPs has used electrodes with somewhat wider spacing than that used here, and with the proximal electrode very close to the cord. Barron and Matthews (1938) reported a maximal PAD potential of 5 mV when the proximal electrode was placed on the root as it left the cord, and the distal electrode ∼10 mm away. In cat, the potential fell by half with every 1.4 mm that the proximal electrode was moved away from the cord. In this study, the cuff electrodes were

located around 5.3 and 6.9 mm away from the cord. This will attenuate the recorded PAD, both because of the greater distance from the cord, and because the closer spacing will give more similar potentials which cancel in the differential recordings. Using Barron and Matthews' estimated numbers would predict a PAD amplitude of around 200 μV. The actual recordings were substantially smaller, around 2 μV (**Figure 2B**), but still detectable above the noise level by averaging. The amplitude difference presumably reflects the many differences between recordings from intact roots in awake monkey compared with roots mounted on hook electrodes in an oil pool in decerebrate cat.

In experiments in anesthetized cats, PAD following peripheral nerve stimulation has an onset around 5–20 ms after the arrival of the volley at the cord (Eccles et al., 1962, 1963b; Manjarrez et al., 2000), which corresponds to the timing of depressed synaptic transmission. In human studies reciprocal inhibition of apparent pre-synaptic origin also begins after a delay in the cord of around 5 ms (Berardelli et al., 1987). The segmental latency of the (DRP) recorded after afferent stimulation here was around 6 ms (**Figure 2A**), which is thus compatible with PAD. By contrast, the duration of this potential was brief compared with previous reports, which often show PAD lasting tens to hundreds of milliseconds. It is possible that rather than reflecting passively conducted PAD itself, this potential reflected the antidromic discharge of axons depolarized by PAD (dorsal root reflex, Eccles et al., 1961b).

Clasically pre-synaptic inhibition is considered to reflect PAD produced by GABAergic axo-axonic synapses (Eccles et al., 1963a; Alvarez, 1998). It has long been known that PAD may be also produced by extracellular potassium accumulation (Kriz et al., 1974; Kremer and Lev-Tov, 1998). The terminal excitability testing used here will be sensitive to modulation in both of these mechanisms. In addition, more recent work has revealed that monoaminergic systems can induce both PAD and depression of synaptic transmission, but with no change in the excitability of intraspinal terminals to antidromic excitation (García-Ramírez et al., 2014). Clearly the methods used here will fail to detect such pre-synaptic inhibition. However, monoaminergic effects on presynaptic inhibition seems to have a slow onset, with changes in synaptic transmission lagging observed changes in DRPs after 5HT application by around 20 s (Figure 5 in García-Ramírez et al., 2014). This would suggest that such mechanisms will also not be capable of temporal modulation on the timescale of tremor cycles, as we found for terminal excitability changes.

Modulation of Pre-synaptic Inhibition

In this report, we have assumed that modulation of the antidromic volley elicited in the dorsal root by intraspinal stimulation reflects increased excitability following depolarization of the afferent terminals, and is a marker of pre-synaptic inhibition (Wall's excitability test; Wall, 1958). However, two other possibilities must also be considered. Orthodromic activity in the sensory afferents will collide antidromic spikes if the two coincide in the brief section of

nerve between the spinal cord and root recording electrode. Modulation of the orthodromic firing rate with task could lead to different fractions of the antidromic spike being collided, and hence to modulation of the antidromic volley. Available data from monkeys performing a wrist flexion-extension task suggests that afferent rates modulate by around 30 discharges per second (Flament et al., 1992). Assuming a collision window equal to the antidromic response latency of the root recording (L ms), this suggests that $30 \times L/1000 \times 100\% = 3 L\%$ of antidromic spikes could collide in this way. **Figure 3D** presents the magnitude of the modulation of dorsal root responses following ISMS as a function of their latency; the diagonal line on that plot indicates modulation of 3 L% expected if collision were the only factor involved. The majority of responses lie above this line, allowing us to conclude that collision with orthodromic spikes cannot explain all of the modulation seen.

Secondly, strong depolarization of the afferent terminals may cause them to spike; these antidromic action potentials will render the terminal inexcitable to stimulation due to the refractory period. Such changes in excitability would still reflect changes in terminal depolarization, although would be opposite in sign to those expected from sub-threshold depolarization. Work in decerebrate cats walking on a treadmill reports antidromic discharge rates of around 35 Hz (Beloozerova and Rossignol, 2004); assuming a refractory period of 1 ms, this would prevent responses only to 3.5% of stimuli. The modulations in **Figure 3D** are generally above this level, and hence this mechanism is likely to be of little consequence for the modulation reported here.

Previous work has demonstrated that pre-synaptic inhibition of cutaneous afferents can modulate in amplitude with different phases of task performance (Seki et al., 2003, 2009), consistent with a role as a "gate" to control afferent inflow during voluntary movement. The present results confirm such task-dependent modulation for a presumed mixed population of muscle and cutaneous afferents. However, based on prior work it was not clear whether pre-synaptic inhibition could modify afferent gain on a faster timescale. On the one hand, the earliest reports showed that changes in monosynaptic reflex amplitude could develop within 10 ms, and recover over around 100 ms (Eccles et al., 1961a); this work used preparations with reduced body temperature, which would plausibly have slowed the time course of effects. Under barbiturate anesthesia at physiological temperatures there are spontaneously occurring deflections in cord-dorsum potentials. Monosynaptic reflexes evoked synchronously with these potentials are markedly potentiated, but return to baseline levels within just 30 ms (see Figure 8 in Manjarrez et al., 2000). Fast timescale modulations in pre-synaptic inhibition therefore seem possible. On the other hand, if pre-synaptic inhibition is elicited by brief trains of stimuli, its duration can be greatly prolonged, with effects often outlasting the stimulus for up to 1 s (Eccles et al., 1961a; Fink et al., 2014). Even following single stimuli, effects up to 300 ms can be seen (Eccles et al., 1963b). Although, the evidence is that pre-synaptic inhibition relies mainly on faster ionotropic (GABA$_A$) receptors (Stuart and Redman, 1992), these slower properties have been suggested to result from asynchronous

release of synaptic transmitter from the axo-axonic contact, or an action on metabotropic ($GABA_B$) receptors (Fink et al., 2014). Such actions would seem incompatible with fast modulation. It is not clear where within this spectrum of observations the action of physiological activity in awake behaving animals should be placed.

The present work demonstrates that, at least in one commonly occurring natural state, pre-synaptic inhibition does not modulate on fast timescales. This negative result assumes special importance in the context of previous findings related to spinal systems and their activity during the ~10 Hz oscillations of physiological tremor. Cortical, brainstem and spinal interneuronal circuits (including pre-motoneuronal interneurons) all modulate their discharge with the tremor cycle (Williams and Baker, 2009; Williams et al., 2009, 2010). The phase relationship of spinal interneurons appears opposite to that of the supra-spinal centers, permitting partial cancellation of oscillatory activity at the motoneuronal level and reduction of oscillatory output. The different phase relationships appear to arise from different responses to sensory input (Koželj and Baker, 2014). Given these other spinal systems which modulate activity with tremor phase, it seemed reasonable that circuits involved in presynaptic inhibition would also modulate. Such modulation, if the phase of maximal inhibition coincided with the peak of tremor-related afferent activity, would act to cancel out oscillations, smoothing the fluctuations in afferent activity and hence reducing tremor amplitude. Yet, surprisingly, such modulation does not seem to exist.

Given the existence of other spinal systems for phase cancelation of oscillations around 10 Hz, we must consider whether some aspect of our experimental design prevented us from detecting a modulation. The most powerful argument that this was not the case is that these results demonstrate clear modulations in spinal terminal excitability with task performance, consistent with previous work (Seki et al., 2003, 2009). Deliberately, intensities yielding responses around half-maximal were used, which should be most sensitive to modulation by excitability changes. Sufficient stimuli were delivered that the signal:noise ratio in response averages was low (**Figure 1C**; see small size of error bars of **Figures 1D, 4C**), arguing against statistical thresholding preventing the detection of small modulations.

One important difference between this experiment and previous work by Seki et al. (2003, 2009) concerns the placement of the recording site. In this work, the cuff electrode was placed on the dorsal root, meaning that recordings would contain a mixture of cutaneous and muscle afferents. By contrast, Seki et al. recorded from the superficial radial nerve, which has only cutaneous fibers. It is known that different categories of afferent exhibit different patterns of PAD in response to sensory or supraspinal inputs (Rudomin and Schmidt, 1999). It is therefore possible that in mixed recordings different afferents

modulated differently with tremor phase, leading to cancellation in the mass record and no discernible modulation. However, similar considerations would be expected to apply to task-related modulation. The fact that task-dependent effects could be seen in many recording sessions, but that tremor-related effects did not occur more than expected by chance, suggests a fundamental difference in the nature of modulation at fast vs. slow timescales.

Although we found modulation of pre-synaptic inhibition during task performance, we cannot provide information on the relative contributions to this effect of afferent input vs. descending control. Sensory afferents (Eccles et al., 1961a) and descending systems (Rudomín et al., 1983; Meunier and Pierrot-Deseilligny, 1998) both control pre-synaptic inhibition and modulate with voluntary movement (Flament et al., 1992; Williams et al., 2010); it is therefore likely that the observed modulations originate from changes in both afferent feedback and descending commands.

Recently, Fink et al. (2014) were able to investigate the contributions of pre-synaptic inhibition to motor control directly in mice using a genetic approach which destroyed pre-synaptic contacts, identified because they specifically express *Gad2*. During forelimb reaching, these mice show oscillatory movements which seem to result from an excessive afferent reflex gain. It would appear that pre-synaptic inhibition is modulated on relatively crude temporal timescales to mark the transition from postural stabilization to movement, with attendant switch from a motor set dominated by reflexes to one under descending voluntary command (Seki et al., 2003, 2009; results of present work on task dependent modulation in **Figure 3**). This switch allows high reflex gain during periods of constant output, but prevents reflexes from interfering with active movement. The results presented here suggest that faster modulations in afferent sensitivity in response to temporal fluctuations in output do not occur.

AUTHOR CONTRIBUTIONS

SB designed the study; SB and FG carried out the experiments; FG performed data analysis and SB and FG wrote the manuscript.

FUNDING

ACKNOWLEDGMENTS

REFERENCES

Alvarez, F. J. (1998). "Anatomical basis for presynaptic inhibition of primary sensory fibers," in *Presynaptic Inhibition and Neural Control*, eds P. Rudomin, R. Romo, and L. Mendell (New York, NY: Oxford University Press), 13–49.

Baker, S. N., Chiu, M., and Fetz, E. E. (2006). Afferent encoding of central oscillations in the monkey arm. *J. Neurophysiol.* 95, 3904–3910. doi: 10.1152/jn.01106.2005

Baker, S. N., and Lemon, R. N. (1998). A computer simulation study of the production of post-spike facilitation in spike triggered averages of rectified EMG. *J. Neurophysiol.* 80, 1391–1406.

Baker, S. N., Olivier, E., and Lemon, R. N. (1997). Coherent oscillations in monkey motor cortex and hand muscle EMG show task-dependent modulation. *J. Physiol.* 501(Pt 1), 225–241. doi: 10.1111/j.1469-7793.1997.225bo.x

Baker, S. N., Pinches, E. M., and Lemon, R. N. (2003). Synchronization in monkey motor cortex during a precision grip task. II. effect of oscillatory activity on corticospinal output. *J. Neurophysiol.* 89, 1941–1953. doi: 10.1152/jn.00832.2002

Barron, D. H., and Matthews, B. H. (1938). The interpretation of potential changes in the spinal cord. *J. Physiol.* 92, 276–321. doi: 10.1113/jphysiol.1938.sp003603

Beloozerova, I. N., and Rossignol, S. (2004). Antidromic discharges in dorsal roots of decerebrate cats. II: studies during treadmill locomotion. *Brain Res.* 996, 227–236. doi: 10.1016/j.brainres.2003.08.067

Berardelli, A., Day, B. L., Marsden, C. D., and Rothwell, J. C. (1987). Evidence favouring presynaptic inhibition between antagonist muscle afferents in the human forearm. *J. Physiol.* 391, 71–83. doi: 10.1113/jphysiol.1987.sp016726

Cheney, P. D., and Preston, J. B. (1976). Classification and response characteristics of muscle spindle afferents in the primate. *J. Neurophysiol.* 39, 1–8.

Conway, B. A., Halliday, D. M., Farmer, S. F., Shahani, U., Maas, P., Weir, A. I., et al. (1995). Synchronization between motor cortex and spinal motoneuronal pool during the performance of a maintained motor task in man. *J. Physiol.* 489(Pt 3), 917–924. doi: 10.1113/jphysiol.1995.sp021104

Eccles, J. C., Eccles, R. M., and Magni, F. (1961a). Central inhibitory action attributable to presynaptic depolarization produced by muscle afferent volleys. *J. Physiol.* 159, 147–166. doi: 10.1113/jphysiol.1961.sp006798

Eccles, J. C., Kozak, W., and Magni, F. (1961b). Dorsal root reflexes of muscle group I afferent fibres. *J. Physiol.* 159, 128–146. doi: 10.1113/jphysiol.1961.sp006797

Eccles, J. C., Magni, F., and Willis, W. D. (1962). Depolarization of central terminals of Group I afferent fibres from muscle. *J. Physiol.* 160, 62–93. doi: 10.1113/jphysiol.1962.sp006835

Eccles, J. C., Schmidt, R. F., and Willis, W. D. (1963b). Depolarization of the central terminals of cutaneous afferent fibers. *J. Neurophysiol.* 26, 646–661.

Eccles, J. C., Schmidt, R., and Willis, W. D. (1963a). Pharmacological Studies on Presynaptic Inhibition. *J. Physiol.* 168, 500–530. doi: 10.1113/jphysiol.1963.sp007205

Elble, R. J., and Randall, J. E. (1978). Mechanistic components of normal hand tremor. *Electroencephalogr. Clin. Neurophysiol.* 44, 72–82. doi: 10.1016/0013-4694(78)90106-2

Fink, A. J., Croce, K. R., Huang, Z. J., Abbott, L. F., Jessell, T. M., and Azim, E. (2014). Presynaptic inhibition of spinal sensory feedback ensures smooth movement. *Nature* 509, 43–48. doi: 10.1038/nature13276

Flament, D., Fortier, P. A., and Fetz, E. E. (1992). Response patterns and postspike effects of peripheral afferents in dorsal root ganglia of behaving monkeys. *J. Neurophysiol.* 67, 875–889.

García-Ramírez, D. L., Calvo, J. R., Hochman, S., and Quevedo, J. N. (2014). Serotonin, dopamine and noradrenaline adjust actions of myelinated afferents via modulation of presynaptic inhibition in the mouse spinal cord. *PLoS ONE* 9:e89999. doi: 10.1371/journal.pone.0089999

Hultborn, H., Meunier, S., Pierrot-Deseilligny, E., and Shindo, M. (1987). Changes in presynaptic inhibition of Ia fibres at the onset of voluntary contraction in man. *J. Physiol.* 389, 757–772. doi: 10.1113/jphysiol.1987.sp016681

Jain, A. K. (2010). Data clustering: 50 years beyond K-means. *Pattern Recognit. Lett.* 31, 651–666. doi: 10.1016/j.patrec.2009.09.011

Koželj, S., and Baker, S. N. (2014). Different phase delays of peripheral input to primate motor cortex and spinal cord promote cancellation at physiological tremor frequencies. *J. Neurophysiol.* 111, 2001–2016. doi: 10.1152/jn.00935.2012

Kremer, E., and Lev-Tov, A. (1998). GABA-receptor-independent dorsal root afferents depolarization in the neonatal rat spinal cord. *J. Neurophysiol.* 79, 2581–2592.

Kriz, N., Sykova, E., Ujec, E., and Vyklicky, L. (1974). Changes of extracellular potassium concentration induced by neuronal activity in the spinal cord of the cat. *J. Physiol.* 238, 1–15. doi: 10.1113/jphysiol.1974.sp010507

Lidierth, M., and Wall, P. D. (1996). Synchronous inherent oscillations of potentials within the rat lumbar spinal cord. *Neurosci. Lett.* 220, 25–28. doi: 10.1016/S0304-3940(96)13231-6

Lippold, O. C. (1970). Oscillation in the stretch reflex arc and the origin of the rhythmical, 8-12 C-S component of physiological tremor. *J. Physiol.* 206, 359–382. doi: 10.1113/jphysiol.1970.sp009018

Loeb, G. E. (1976). Decreased conduction velocity in the proximal projections of myelinated dorsal root ganglion cells in the cat. *Brain Res.* 103, 381–385. doi: 10.1016/0006-8993(76)90810-6

Lomelí, J., Quevedo, J., Linares, P., and Rudomin, P. (1998). Local control of information flow in segmental and ascending collaterals of single afferents. *Nature* 395, 600–604. doi: 10.1038/26975

Manjarrez, E., Rojas-Piloni, J. G., Jimenez, I., and Rudomin, P. (2000). Modulation of synaptic transmission from segmental afferents by spontaneous activity of dorsal horn spinal neurones in the cat. *J. Physiol.* 529(Pt 2), 445–460. doi: 10.1111/j.1469-7793.2000.00445.x

Marks, W. B., and Loeb, G. E. (1976). Action currents, internodal potentials, and extracellular records of myelinated mammalian nerve fibers derived from node potentials. *Biophys. J.* 16, 655–668. doi: 10.1016/S0006-3495(76)85719-0

Marsden, C. D., Meadows, J. C., Lange, G. W., and Watson, R. S. (1969). The role of the ballistocardiac impulse in the genesis of physiological tremor. *Brain* 92, 647–662. doi: 10.1093/brain/92.3.647

Meunier, S., and Pierrot-Deseilligny, E. (1998). Cortical control of presynaptic inhibition of Ia afferents in humans. *Exp. Brain Res.* 119, 415–426. doi: 10.1007/s002210050357

Mitchell, W. K., Baker, M. R., and Baker, S. N. (2007). Muscle responses to transcranial stimulation in man depend on background oscillatory activity. *J. Physiol.* 583, 567–579. doi: 10.1113/jphysiol.2007.134031

Rudomín, P., Jimenez, I., Solodkin, M., and Duenas, S. (1983). Sites of action of segmental and descending control of transmission on pathways mediating PAD of Ia- and Ib-afferent fibers in cat spinal cord. *J. Neurophysiol.* 50, 743–769.

Rudomin, P., Lomelí, J., and Quevedo, J. (2004). Differential modulation of primary afferent depolarization of segmental and ascending intraspinal collaterals of single muscle afferents in the cat spinal cord. *Exp. Brain Res.* 156, 377–391. doi: 10.1007/s00221-003-1788-7

Rudomin, P., and Schmidt, R. F. (1999). Presynaptic inhibition in the vertebrate spinal cord revisited. *Exp. Brain Res.* 129, 1–37. doi: 10.1007/s002210050933

Salenius, S., Portin, K., Kajola, M., Salmelin, R., and Hari, R. (1997). Cortical control of human motoneuron firing during isometric contraction. *J. Neurophysiol.* 77, 3401–3405.

Seki, K., Perlmutter, S. I., and Fetz, E. E. (2003). Sensory input to primate spinal cord is presynaptically inhibited during voluntary movement. *Nat. Neurosci.* 6, 1309–1316. doi: 10.1038/nn1154

Seki, K., Perlmutter, S. I., and Fetz, E. E. (2009). Task-dependent modulation of primary afferent depolarization in cervical spinal cord of monkeys performing an instructed delay task. *J. Neurophysiol.* 102, 85–99. doi: 10.1152/jn.91113.2008

Shinoda, Y., Yamaguchi, T., and Futami, T. (1986). Multiple axon collaterals of single corticospinal axons in the cat spinal cord. *J. Neurophysiol.* 55, 425–448.

Soteropoulos, D. S., Williams, E. R., and Baker, S. N. (2012). Cells in the monkey ponto-medullary reticular formation modulate their activity with slow finger movements. *J. Physiol.* 590, 4011–4027. doi: 10.1113/jphysiol.2011.225169

Stuart, G. J., and Redman, S. J. (1992). The role of GABAA and GABAB receptors in presynaptic inhibition of Ia EPSPs in cat spinal motoneurones. *J. Physiol.* 447, 675–692. doi: 10.1113/jphysiol.1992.sp019023

Wall, P. D. (1958). Excitability changes in afferent fibre terminations and their relation to slow potentials. *J. Physiol.* 142, 1–21. doi: 10.1113/jphysiol.1958.sp005997

Wessberg, J., and Vallbo, A. B. (1995). Coding of pulsatile motor output by human muscle afferents during slow finger movements. *J. Physiol.* 485, 271–282. doi: 10.1113/jphysiol.1995.sp020729

Williams, E. R., and Baker, S. N. (2009). Renshaw cell recurrent inhibition improves physiological tremor by reducing corticomuscular coupling at 10 Hz. *J. Neurosci.* 29, 6616–6624. doi: 10.1523/JNEUROSCI.0272-09.2009

Williams, E. R., Soteropoulos, D. S., and Baker, S. N. (2009). Coherence between motor cortical activity and peripheral discontinuities during slow finger movements. *J. Neurophysiol.* 102, 1296–1309. doi: 10.1152/jn.90996.2008

Williams, E. R., Soteropoulos, D. S., and Baker, S. N. (2010). Spinal interneuron circuits reduce approximately 10-Hz movement discontinuities by phase cancellation. *Proc. Natl. Acad. Sci. U.S.A.* 107, 11098–11103. doi: 10.1073/pnas.0913373107